NREL
NATIONAL RENEWABLE ENERGY LABORATORY

A Comparison of the Dynamic Wake Meandering Model, Large-Eddy Simulation, and Field Data at the Egmond aan Zee Offshore Wind Plant

Preprint

M.J. Churchfield and P.J. Moriarty
National Renewable Energy Laboratory

Y. Hao and M.A. Lackner
University of Amherst

R. Barthelmie
Cornell University

J. Lundquist
University of Colorado at Boulder

G. S. Oxley
Vestas Wind Systems A/S

To be presented at the AIAA Science and Technology Forum and Exposition 2015
Kissimmee, Florida
January 5–9, 2015

Conference Paper
NREL/CP-5000-63321
December 2014

Contract No. DE-AC36-08GO28308

This report is available at no cost from the National Renewable Energy Laboratory (NREL) at www.nrel.gov/publications.

Available electronically at http://www.osti.gov/scitech

Available for a processing fee to U.S. Department of Energy and its contractors, in paper, from:

U.S. Department of Energy
Office of Scientific and Technical Information
P.O. Box 62
Oak Ridge, TN 37831-0062
phone: 865.576.8401
fax: 865.576.5728
email: mailto:reports@adonis.osti.gov

Available for sale to the public, in paper, from:

U.S. Department of Commerce
National Technical Information Service
5285 Port Royal Road
Springfield, VA 22161
phone: 800.553.6847
fax: 703.605.6900
email: orders@ntis.fedworld.gov
online ordering: http://www.ntis.gov/help/ordermethods.aspx

Cover Photos: (left to right) photo by Pat Corkery, NREL 16416, photo from SunEdison, NREL 17423, photo by Pat Corkery, NREL 16560, photo by Dennis Schroeder, NREL 17613, photo by Dean Armstrong, NREL 17436, photo by Pat Corkery, NREL 17721.

NREL prints on paper that contains recycled content.

A Comparison of the Dynamic Wake Meandering Model, Large-Eddy Simulation, and Field Data at the Egmond aan Zee Offshore Wind Plant

Matthew J. Churchfield,* and Patrick J. Moriarty*
National Renewable Energy Laboratory, Golden, Colorado, 80401, USA

Yujia Hao† and Matthew A. Lackner ‡
University of Massachusetts Amherst, Amherst, Massachusetts, 01003, USA

Rebecca Barthelmie§
Cornell University, Ithaca, New York, 14853, USA

Julie K. Lundquist¶
University of Colorado, Boulder, Boulder, Colorado, 80309, USA

Gregory S. Oxley‖
Vestas Wind Systems A/S, Aarhus, 8200, Denmark

The focus of this work is the comparison of the dynamic wake meandering model and large-eddy simulation with field data from the Egmond aan Zee offshore wind plant composed of 36 3-MW turbines. The field data includes meteorological mast measurements, SCADA information from all turbines, and strain-gauge data from two turbines. The dynamic wake meandering model and large-eddy simulation are means of computing unsteady wind plant aerodynamics, including the important unsteady meandering of wakes as they convect downstream and interact with other turbines and wakes. Both of these models are coupled to a turbine model such that power and mechanical loads of each turbine in the wind plant are computed. We are interested in how accurately different types of waking (e.g., direct versus partial waking), can be modeled, and how background turbulence level affects these loads. We show that both the dynamic wake meandering model and large-eddy simulation appear to underpredict power and overpredict fatigue loads because of wake effects, but it is unclear that they are really in error. This discrepancy may be caused by wind-direction uncertainty in the field data, which tends to make wake effects appear less pronounced.

*Senior Engineer, National Wind Technology Center, 15013 Denver West Parkway, AIAA Member.
†Graduate Research Assistant, Department of Mechanical and Industrial Engineering, 160 Governors Drive.
‡Assistant Professor, Department of Aerospace Engineering, 160 Governors Drive, AIAA Member.
§Professor, Sibley School of Mechanical and Aerospace Engineering, College of Engineering, Upson Hall.
¶Assistant Professor, Department of Atmospheric and Oceanic Sciences, 311-UCB.
‖Plant Flow Modeling Specialist, Plant Siting and Forecasting, Service Engineering, Hedeager 44.

I. Introduction

The ability to accurately model wind plant performance continues to gain importance. Not only does "performance" imply power production, it also increasingly implies wind turbine structural loading. Both power and loads are important drivers of the cost of energy, so having a reliable way to model performance is important. Also, as interest in wind-plant-level control systems grows, having the ability to model power and loads is important because such control systems often aim to optimize both. Central to modeling wind plant performance is the ability to accurately represent wind plant aerodynamics that are dominated by the complex, unsteady, three-dimensional wind turbine wakes, atmospheric turbulence, and their interactions.

In this work, we compare the ability of two very different models for wind plant aerodynamics, the dynamic wake meandering (DWM) model and large-eddy simulation (LES), to simulate the operational Egmond aan Zee (OWEZ) offshore wind plant, for which comprehensive field data are available. The DWM model solves the axisymmetric thin-shear-layer equation for a wind turbine wake, and then, given a pregenerated turbulent field, perturbs the wake with that turbulence in the lateral and horizontal directions in a time-varying fashion to mimic wake meandering. The DWM model can be run on a modern laptop, assuming the inflow turbulence is generated with a computationally inexpensive method (e.g, a stochastic turbulence generator). On the other hand, LES is a type of computational fluid dynamics (CFD) that solves the full nonlinear Navier-Stokes equations. It solves those equations in a filtered form so that it directly resolves the larger energy-containing scales of turbulence and models the effects of the smaller scales. The turbulent inflow wind is often generated in a separate precursor atmospheric LES, and the turbine wakes are commonly produced by introducing actuator disks or lines into the flow field. Unlike the DWM model that completely models wake meandering, LES directly solves for wake meandering dynamics using the Navier-Stokes equations. LES can naturally account for atmospheric stability, which significantly affects wake behavior, through the inclusion of a buoyancy term in the vertical momentum equation. LES is expensive requiring hundreds or thousands of computer cores over a few days to simulate a 10-minute period of the flow through a full wind farm. Both the DWM model and LES can be coupled with wind turbine structural and system dynamic models to then examine wind turbine power production, mechanical loads, and control system response.

LES is valuable in that the uncertainties of modeling are minimized because it directly solves the Navier-Stokes equations for the larger scales of turbulence and models the effects of only the small scales. If set up correctly with proper boundary conditions and forcings, its high spatial and temporal resolution makes it a great tool that complements field observations. However, because of its expense, it should be directed at specific cases to examine them in detail.

There is also a strong need for accurate wind plant aerodynamics tools that capture unsteady behavior but that are computationally inexpensive. The DWM model is aimed at this category. Originally introduced by Larsen et al.[1,2] in 2007, it is a relatively new model. It is unique from other wind turbine wake models, such as the commonly used Park model[3,4] or eddy viscosity model[5] because it accounts for wake meandering, an observed unsteady phenomena that is discussed by Bingöl et al.[6] and Trujillo et al.[7] As wakes convect downwind, they meander laterally and horizontally. This unsteadiness not only causes power fluctuations in downstream waked turbines, but also significant unsteady mechanical loads. Older wake models, such as the Park model, do not account for any unsteadiness, but only attempt to compute the mean wake deficit. For loads analysis, the International Electrotechnical Commission (IEC) standards that govern wind turbine design specify that an increased turbulence intensity is applied[8] (see Annex D of IEC standard 61400-1), but this uniformly elevated turbulence level lacks the structure of a coherent meandering wake, and the DWM model attempts to address this deficiency.

Although, the DWM model was compared to field data from the OWEZ site by Larsen et al.,[9] we also compared with OWEZ data using our own implementation of the DWM model. Currently, the DWM model has been coupled with the National Renewable Energy Laboratory's (NREL) FAST[10] wind turbine structural and system dynamics code. This coupling is well documented in the work by Hao et al.,[11] and the coupled DWM model/FAST tool will become part of NREL's Simulator fOr Wind Farm Applications (SOWFA) tool set.[12] We also performed LES using NREL's OpenFOAM-based flow solver, which can also be coupled to FAST and is another component of SOWFA.

This paper is outlined as follows. Section II gives an overview of the OWEZ site; Section III describes our LES model and the DWM model in more detail; Section IV shows and discusses the comparisons between the DWM model, LES, and field data; and SectionV provides our conclusion.

II. OWEZ Site Description

The OWEZ wind plant, which is roughly 10 km off the shore of The Netherlands, consists of 36 Vestas V90-3.0-MW wind turbines sitting atop 70-m towers. As shown in Figure 1, the turbines are situated in four major rows. The turbine spacing within a row is roughly 7.1 rotor diameters (D) and the spacing between rows is roughly 11.1 D. An exception to this occurs between turbines 16 and 17, 24 and 25, and 31 and 32 in which the spacing is increased to 11.4 D. Turbines 7 and 8 were fully instrumented for mechanical loads measurements. A meteorological mast with various wind and water sensors, including sonic anemometers useful for measuring inflow turbulence quantities, is situated to the south-southwest of turbine 8. The meteorological mast is useful for quantifying the wind plant inflow when the winds are from the south-southeast through the west-northwest. For the other directions, the turbines themselves must be used as wind speed sensors, either employing the turbines' nacelle anemometers or the power curve.

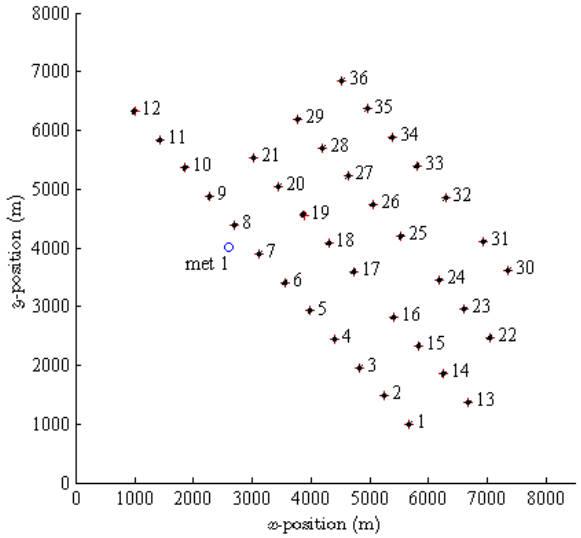

Figure 1. The layout of the OWEZ wind plant. The positive y-coordinate is north; the positive x-coordinate is east.

III. Model Descriptions

III.A. Dynamic Wake Meandering Model

As with the implementation of Larsen et al.,[1,2] our implementation of the DWM model consists of two submodels as described by Hao et al.:[11] 1) a model of the quasi-steady wake deficit, and 2) a model of the downstream stochastic wake meandering process.

The quasi-steady wake deficit model is similar to that of Ainslie,[5] in which the steady, axisymmetric, thin-shear-layer form of the Navier-Stokes equations are solved with an eddy-viscosity turbulence model. This piece of the model computes the "base" wake, which decays and expands with downstream distance. The quasi-steady wake deficit model also includes the strain-rate contribution from the vertical shear of the atmospheric boundary layer, an effect recently proposed by Keck et al.[13]

The second part of the model describes the large-scale lateral and vertical meandering process of the turbine wake. In the DWM model, it is assumed that this meandering is driven by large-scale turbulent structures in the atmospheric boundary layer. First, a turbulent inflow is pregenerated. Usually, it is created by a stochastic turbulence generator. In this case, we used NREL's TurbSim,[14] but it could also be generated by LES. Then, the quasi-steady wake is treated as a passive tracer that is perturbed laterally and vertically using the pregenerated turbulence time history. Taylor's frozen turbulence hypothesis is used, and the wake is convected at some percentage of the free stream speed. The DWM model is distinguished from other wake models by its ability to capture the time-dependent physics present in wind turbine wakes. As a consequence, both wind turbine loads and power production can be predicted at the same time.

In this study, the DWM model is implemented in NREL's FAST code.[10,11] FAST is a wind turbine

structural and system dynamics tool. This implementation of the DWM is run in a sequential fashion in which the most upwind turbines are simulated and subjected to non-waked turbulent inflow winds generated with TurbSim.[14] Actual Vestas V90 design and control information is used in the FAST model. The mean axial induction factors of these upwind turbines are used to generate the DWM model "base" wake, which is meandered using the TurbSim flow field. Then, the next set of downwind turbines are subjected to the TurbSim inflow with the DWM model wake superimposed upon it. Mean axial induction factors of these next turbines are extracted so that the DWM model can be computed for these turbines' wakes. The process continues deeper into the wind plant until the entire plant is simulated. It is important to note that although the TurbSim inflow field is turbulent, the mean wind speed and direction upon which the turbulence is superimposed is fixed in time. This is different than in the real atmosphere in which the larger spatial and temporal wind scales are never perfectly time invariant.

III.B. Large-Eddy Simulation

The LES tool we used in this work is described in detail by Churchfield et al.,[15] and is built upon the OpenFOAM computational fluid dynamics toolbox,[16] which is a free, open-source set of libraries for solving complex partial differential equations. The code is second-order accurate in space and time and uses the unstructured finite-volume formulation. Because the solver is meant to compute wind plant aerodynamics that lie within the atmospheric boundary layer, buoyancy effects of atmospheric stratification are incorporated through the inclusion of a Boussinesq buoyancy term in the vertical momentum equation. The unstructured mesh capability allows for variable resolution within the domain. Typically, the atmospheric flow away from the turbines is computed on a mesh of uniform roughly 10-m resolution. The resolution is increased to 1–2 m around the turbines and in their wakes to capture relevant wake details. We commonly use the Lagrangian-averaged dynamic Smagorinsky subgrid-scale (SGS) model.[17] When computing wind plant flow, the inflow boundary conditions are from a separate precursor LES without turbines.

The turbines were modeled as rotating actuator lines following Sørensen and Shen.[18] The turbine blades were modeled as lines of force along the blade. Airfoil look-up tables were used to compute the force along the line. The line forces were then applied to the flow field as body forces in the momentum equations. The rotor speed was controlled by a simulated generator-torque controller and blade-pitch controller. In this case, we used blade, airfoil, and tip-speed ratio data from the actual Vestas V90.

An offshore wind plant case in which our LES tool has been validated is that of the operational Lillgrund offshore plant composed of 48 2.3-MW turbines.[19]

In this study, we simulated only one case with LES because of the relatively high compute cost and lack of time to perform more cases. Although only one case was computed, it yielded a wealth of unsteady flow and turbine performance information. In that case, a precursor LES was performed to create the inflow winds that have a turbulence intensity of 4.1% and wind speed of 9 m/s from the 315° wind direction. In the precursor LES, the mean is defined as the horizontal average of the wind field each time step. The solver is set up so that this mean wind speed and direction is time invariant. This allows for more local wind direction and speed variation than with the TurbSim-generated DWM model inflow since the LES precursor domain is kilometers in scale and can resolve much larger spatial scales, but it still cannot represent the even larger scales that change over time that exist in the real atmosphere. The mean wind direction is not directly down the main row direction, but oblique to the row by nearly 4°. Instantaneous snapshots of the unsteady velocity field from this simulation are shown in Figure 2.

IV. Results

From the start of this work, we were concerned about the effects of atmospheric stability on power production and mechanical loads. Our initial analysis of the data, though, showed the dependence on stability, as classified by Richardson number (Ri) or Obukhov length (L), to be unclear. However, we found when we examined the data binned by inflow turbulence intensity (based on horizontal velocity), a clear dependence of power and loads on that quantity. We also found that for the OWEZ site, for a given atmospheric stability level, there may exist a range of turbulence intensities, as shown in Figure 3. We expected that with stable atmospheric conditions, the turbulence intensity would be lower than with unstable conditions. Instead, we saw that the lowest turbulence intensity that occurs for a given stable Obukhov length is lower than that for a given unstable Obukhov length, but both the stable and unstable

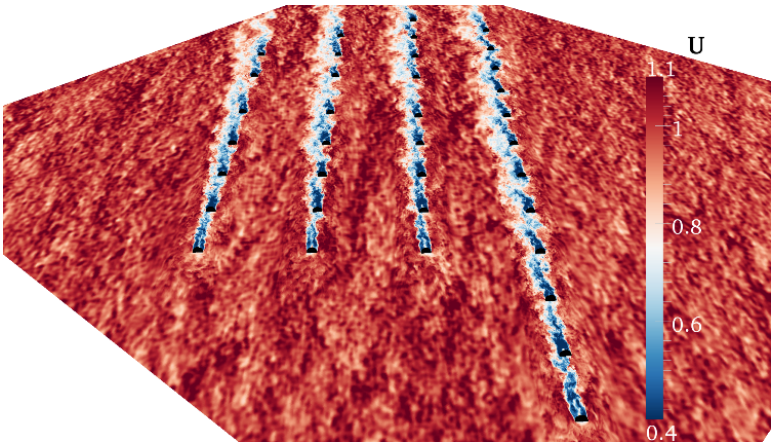

(a)

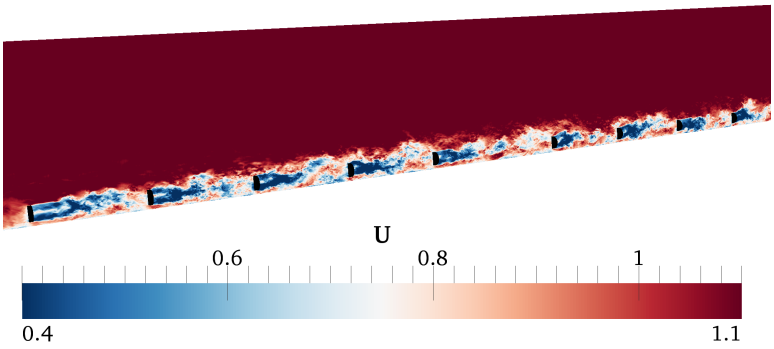

(b)

Figure 2. The instantaneous velocity field of the OWEZ wind plant from LES in a horizontal plane at hub height (a), and in a vertical plane aligned with row 2 (b). The simulated mean wind direction is nearly 4° offset from the main row direction. The black disks denote the location of the 36 turbine rotors.

Obukhov lengths have a full range of turbulence intensities associated with them. For this reason, we focused on examining the effect of turbulence intensity on loads and power instead of stability. We felt it made sense to do this: Richardson number and Obukhov length are measures of stability, not turbulence level; wakes, and hence wake-induced power and load effects, are affected by the turbulence directly, not the stability level. Other measures of turbulence not examined in this study include turbulence intensity based on vertical fluctuations, turbulent kinetic energy (or turbulence intensity based on all three components of velocity fluctuation), and Kelley's coherent turbulent kinetic energy.[20] These other turbulence quantities should be examined in future work.

Although we are interested in wind-plant performance over the entire wind rose, wind-speed range, and turbulence-intensity range, that parameter space is very large and out of the scope of this paper. We were able to simulate many more cases with the DWM model than with LES because of the DWM model's relative inexpensiveness. With the DWM model, all simulations were at 9 m/s, a wind speed in which the wake deficit is strong. We split the data into different turbulence intensity ranges and simulate all ranges with the DWM model. For the 4–6% turbulence intensity range, we simulated the entire wind direction range with the DWM model, but for all other turbulence intensity ranges, we focused on the wind direction range about the main row direction, 318.7°. Because of its high cost, we only simulated one case with LES, but plan to simulate more cases in the future. The large amount of wake data and blade loading data sampled at high frequency from the LES case will be used to further refine the DWM model. A summary of the cases simulated is shown in Table 1.

The field data consists of 10-minute statistics over three years. Each DWM model simulation was run for 350 s, the statistics of which were found to be converged, alleviating the need to run the DWM model

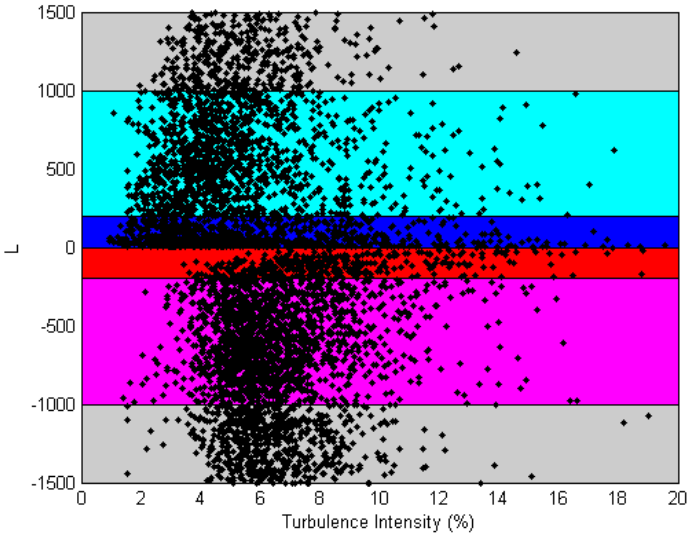

Figure 3. A plot of turbulence intensity versus Obukhov length, L. The different colored backgrounds indicate the different stability classes used in this study based on Obukhov length (red - unstable; magenta - slightly unstable; gray - neutral; cyan - slightly stable; blue - stable).

Table 1. Ranges of turbulence intensity, wind direction, and wind speed simulated with the DWM model and LES and compared to field data.

Field Data			DWM Model			LES		
TI (%)	Direction (°)	Speed (m/s)	TI (%)	Direction (°)	Speed (m/s)	TI (%)	Direction (°)	Speed (m/s)
2–4	0–360	8–10	3	310–330	9	—	—	—
4–6	0–360	8–10	4.5	0–360	9	4.1	315	9
6–8	0–360	8–10	7.5	310–330	9	—	—	—
8–10	0–360	8–10	9	310–330	9	—	—	—
10–12	0–360	8–10	11	310–330	9	—	—	—

for the full 10 minutes. The LES was run for more than 10 minutes, but statistics were taken from the last 10 minutes of the simulation.

We focused on both power and loads, so the results are split into two subsections. For power, we examined the global wind plant efficiency and relative power production of the turbines within the four main rows. For loads, we focused solely on blade-root out-of-plane (BR-OOP) bending moment.

IV.A. Power and Efficiency

In comparing wind plant power and efficiency field data to simulation data, we often plotted these quantities versus wind direction. The field data is comprised of 3 years of 10-minute averages, and there is significant scatter in the data. To better understand the field data dependence on wind direction, it is binned in 5° bins. Additionally, the field data direction measurement contains uncertainty, as discussed by Gaumond et al.[21] When examining power and efficiency in a turbine-row-aligned direction, the wind direction uncertainty in the field data makes the wake effects appear weaker. For example, if the mean wind direction of a single 10-minute data point was recorded as row aligned, but the actual direction was offset from the row direction by a few degrees, or the wind swept across the row direction over the 10 minutes, the efficiency appears higher than if the wind were actually row aligned.

It quickly became apparent that we could not simply compare the simulation output to the field data without accounting for the fact that the field data contains wind direction uncertainty. Therefore, we used the method of Gaumond et al.[21] in which the time-averaged simulation data as a function of wind direction is convolved with a Gaussian function of wind direction centered on the wind direction of interest. This means that for each wind direction, multiple simulations are required at and around the wind direction of

interest. The convolution is done for each wind direction. The convolution replaces data at a specific wind direction with a Gaussian-weighted average of that data point and the surrounding data points. Gaumond et al. explain that the Gaussian width, σ_a, is directly related to the uncertainty of the wind direction within the 10-minute period over which the average was taken. That wind direction uncertainty can be measured by the standard deviation of the wind direction over the 10-minute period.

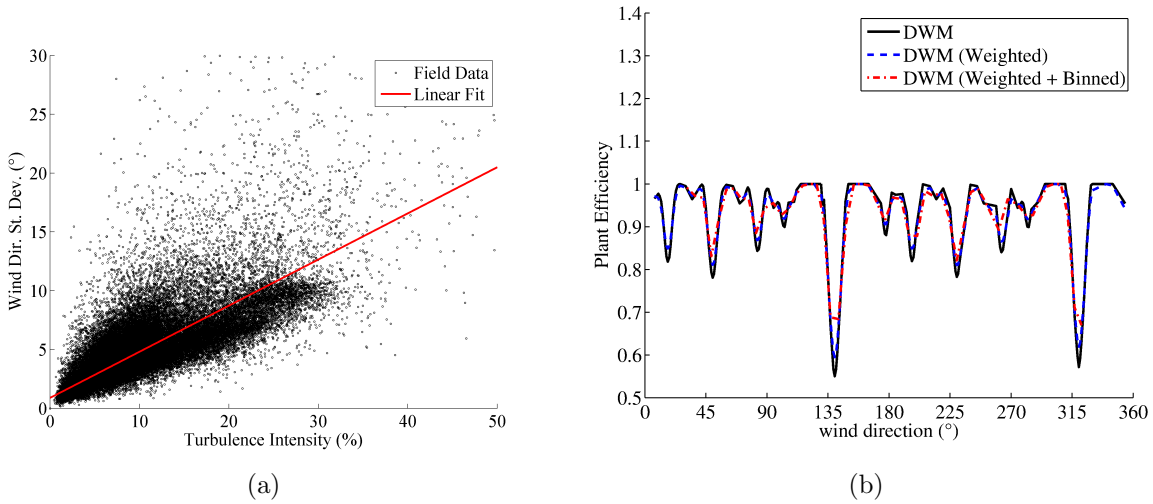

(a) (b)

Figure 4. (a) The black symbols show the wind direction standard deviation versus turbulence intensity based on 10-minute samples taken from a sonic anemometer on the meteorological mast at 70 m above the surface, which is the turbine hub height. The red line is the linear fit of the data. (b) The effect of applying the Gaussian weighting and wind-direction-bin averaging to the DWM model data.

Because we often examined the data as a function of wind direction, but binned it by turbulence intensity, and turbulence intensity affects the standard deviation of wind direction, we plotted 10-minute derived standard deviation of wind direction versus turbulence intensity from meteorological mast data taken at hub height over the three years of available data. We then performed a linear fit on this data to define a function of wind direction standard deviation versus turbulence intensity. The data and the linear fit is shown in Figure 4 (a). The wind direction standard deviation as a function of turbulence intensity was used as the Gaussian-weighting function width, σ_a. The linear fit is given by

$$\sigma_a = 0.88 + 39.23\text{TI}, \tag{1}$$

where TI is turbulence intensity. For example, a 5% turbulence intensity yields $\sigma_a = 2.84°$.

Because of the scatter in the field data, we wind-direction-bin averaged the data, so the same must be done to the Gaussian-weighted simulation data to make a useful comparison. The effect of bin-averaging is to cause wake effects to appear further reduced. To illustrate the effect of Gaussian weighting and wind-direction-bin averaging on wind plant efficiency, we show an example efficiency versus wind direction plot in Figure 4 (b). That plot shows the raw DWM model output, then the effect of Gaussian weighting, and finally the effect of Gaussian weighting and wind-direction-bin averaging. For each successive level of processing, the gradients in the data are smoothed.

We examined wind plant efficiency in Figure 5. Wind plant efficiency is the total power generated by the wind plant divided by the power achieved if all 36 turbines were in the freestream and not subject to wake effects. Freestream power is defined as the mean of the 10-minute time-averaged power generated by the leading turbines. Different turbines are considered leading turbines depending on the freestream wind direction, but for the 315° wind direction, for example, the leading turbines are 12, 21, 29, and 36 (see Figure 1). Each plot in Figure 5 is for a different turbulence intensity range. The blue symbols represent different data points from the field data that fit within the 8–10 m/s wind speed bin and the different turbulence intensity bins. The black line is the wind-direction-bin average of these field data points within 5° bins, but portions of the line are omitted if fewer than 3 data samples occupy a given wind-direction bin. The red and green symbols represent DWM model and LES data points, respectively, with no direction-uncertainty Gaussian weighting. The cyan line is the 5° wind-direction-bin average of the Gaussian-weighted DWM model data. The vertical black dotted lines indicated wind directions aligned with a turbine row, and the turbine spacing for each of these row directions is given in terms of rotor diameters.

Decreases in efficiency observed in the field data are clearly seen along row directions, especially the 7.1 D direction of 318.7°. Very little field data is available when wind is aligned with this row from the opposite direction. For the lowest turbulence intensity bin, 2%–4%, individual 10-minute average data points show that the efficiency drops to as low as 0.5 for the 318.7°-direction (but the 5°-bin average is roughly 0.65). As the turbulence-intensity bin level is increased, this minimum efficiency increases. For example, for the 8%–10% turbulence intensity bin, the field data bin average efficiency for the 318.7° direction is near 0.8. For directions in which the spacing is larger, the drop in efficiency is much smaller. For example, in the 2%–4% turbulence intensity bin, the 11.1 D spacing efficiency is roughly 0.85, compared to 0.65 for the 7.1 D spacing.

The DWM model reflects the field data reasonably well. Decreases in efficiency are observed when wind is aligned with rows, and the efficiency is lower for small spacings. The individual DWM model data points lie well within the scatter of the field data. The individual DWM model data points, though, show considerably less efficient wind plant performance when wind is perfectly row aligned, but show higher performance a few degrees from perfectly aligned. The weighted and bin-averaged DWM model data agree reasonably well with the bin-averaged field data. The deficit at the 318.7° wind direction is usually predicted within 5%–8%; however, there is so much scatter in the field data that assigning a percent difference between the DWM model and field data is not an accurate measure of model performance. With this much field data scatter, it is not clear how to judge model performance.

In regions of the wind rose in which wake effects are not present, the DWM model predicts the efficiency to rise to 1. The field data has considerable scatter above and below 1, but the wind-direction-bin average is below 1. The values that are less than 1 could be present because there may be wind direction and speed variations across the wind plant that allow for waking in some parts of the plant. For example, when the meteorological mast-measured direction is one in which wake effects should be absent, the turbines near the meteorological mast likely experience that non-waking wind direction, but with increasing distance from the mast, wind direction uncertainty increases and there is a higher probability that the wind direction does cause some degree of waking. The greater than 1 values may be present because of wind speed variations across the farm such that the majority of the wind plant is experiencing higher wind speeds than the freestream turbines. The DWM model, though, does not model such stochastic variations across the wind plant; all turbines are subject to the same inflow wind file generated by TurbSim.[14]

As only one LES case was run due to its expense, there is one LES data point on the 4%–6% turbulence intensity plot at a wind direction of 315°. Qualitatively, it lies well within the field data scatter, and it predicts a slightly lower efficiency than the DWM model, which may be due to the lower turbulence intensity of the LES inflow compared to the DWM model inflow. Because there is only one LES data point, no Gaussian weighting or bin averaging could be performed.

It is also useful to look at the power produced by individual turbines relative to the freestream turbines. Figure 6 shows the relative power of each turbine in each of the four rows when the wind is row aligned at 318.7° and the turbulence intensity is 4%–6%. For the field data, the mean of all 10-minute averages that lie within the row direction ±1° is shown, and the gray shaded area shows ±1 standard deviation of this collection of 10-minute average for each turbine. Because the DWM model was not run for three years like the field data, but rather each distinct condition was simulated once, we do not show standard deviation of the DWM model data. However, the DWM model data is weighted with the Gaussian function, as discussed above, and wind-direction-bin averaged using a ±1° bin as with the field data.

In all cases, the DWM model underpredicted relative power (i.e., it overpredicts wake losses). However, the DWM model results lie well within ±1 standard deviation of the field data. We do not feel that this is a clear indicator that the DWM model is actually performing poorly. We believe that the wind direction uncertainty in the field data, which is likely larger than the bin width we used, causes the wake losses to appear artificially weak. Although we tried to account for the wind direction uncertainty in our DWM model results using the method of Gaumond et al.,[21] it is not clear that we truly represented that uncertainty. We also found that the DWM model results are highly sensitive to wind-direction-bin averaging width. Using a bin width of ±2° significantly decreased the apparent wake losses, bringing the DWM model results more in line with the field data. Lastly, the DWM model simulations shown here were at a single freestream turbulence intensity of 4.5%, but the field data is comprised of measurements when turbulence intensity is anywhere between 4% and 6%. The 4.5% of the DWM model calculation is below the midpoint of the field data turbulence intensity range, and for lower turbulence intensity, we expect greater power deficits.

Although the magnitude of the DWM model-predicted relative power is shown to be too low, the DWM

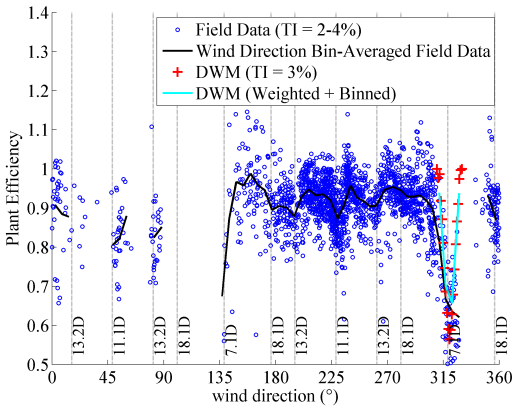

(a) TI = 2-4%

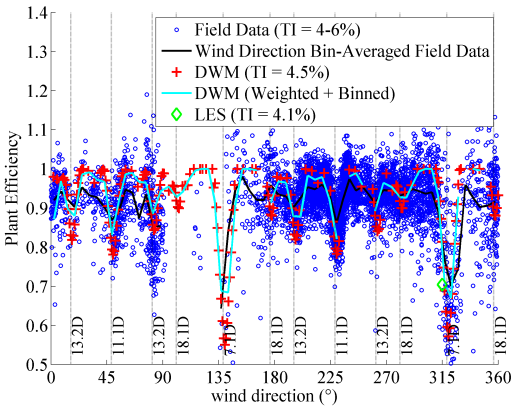

(b) TI = 4-6%

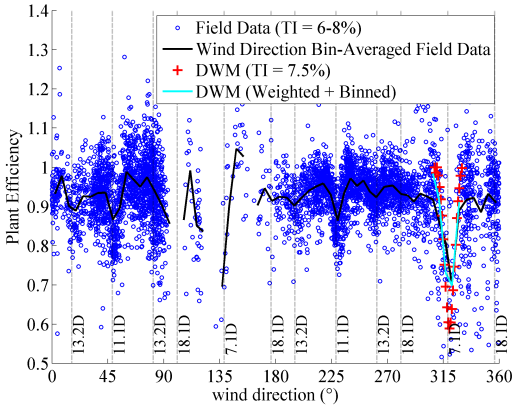

(c) TI = 6-8%

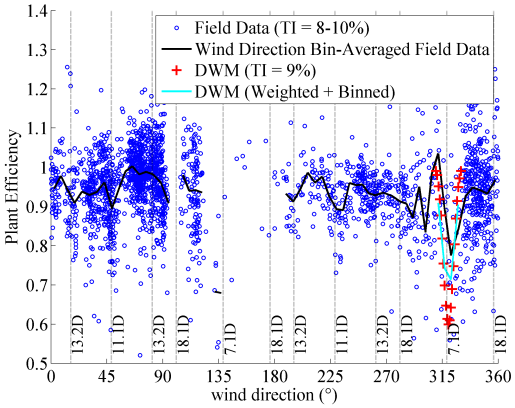

(d) TI = 8-10%

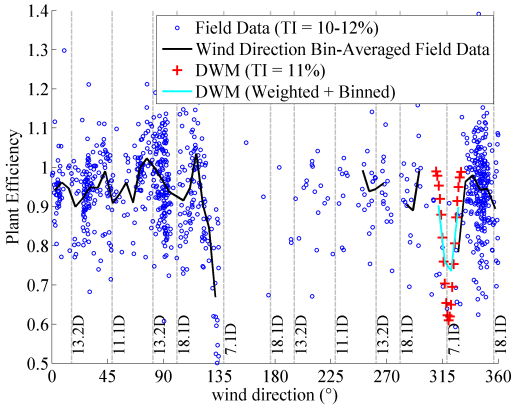

(d) TI = 10-12%

Figure 5. Plots of wind plant efficiency versus wind direction for different turbulence intensity levels.

model predicts important features of the power losses down the row. For example, it predicts a drop in power in the second turbine in a row followed by some degree of recovery. This behavior is commonly seen in field data and is clearly visible in the field data for rows 1 and 4. It is not visible in the field data from rows 2 and 3, and one possible reason may be that the turbines are not located exactly as stated. If there is relatively minor lateral offset of the second turbine in the row, the dramatic power decrease for the second turbine may not occur. The DWM model also predicts the power recovery at turbines 16, 24, and 31 because of the increased spacing between those turbines and the next turbines upstream.

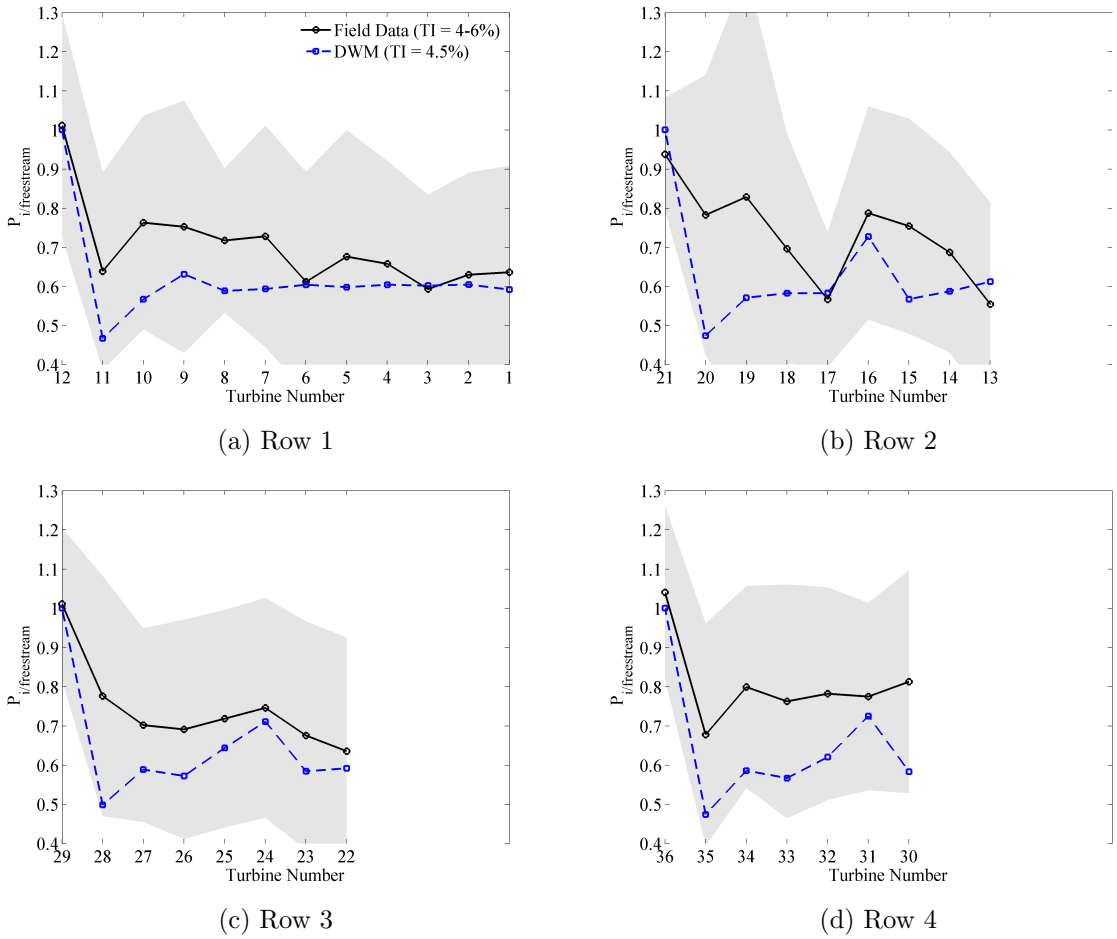

Figure 6. Mean power of each turbine in each row relative to the average of the power produced by the freestream turbines (12, 21, 29, 36). The black solid line is the bin-average (±1°) of 10-minute mean field data. The gray shading denotes ±1 standard deviation of the field data. The blue dashed line is the Gaussian-weighted and bin-averaged (±1°) 350-s mean DWM model data. The wind direction is row aligned at 318.7° and the turbulence intensity is 4%–6%.

Because having the mean wind direction perfectly row-aligned is a rare situation, we also examined the situation when the wind is a few degrees from row-aligned. Figure 7 shows relative power down turbine rows when the wind is from 315°, which is nearly 4° from row-aligned. Again, the turbulence intensity bin shown is 4%–6%. Also in this case, the LES results are included because that simulation was from 315°, but no bin averaging or Gaussian weighting could be done on the LES data because only one wind direction was simulated.

In this case, the DWM model-predicted relative power is generally underpredicted, but not as much as in the row-aligned case. In fact, for rows 1–3, there are turbines in which the DWM model-predicted power is higher than the field data. Again, the sharp decrease in power at the second turbine in each row is predicted with the DWM model, which is also shown in the field data for rows 1 and 4. The LES data is significantly lower than the field data and the DWM model data, but no bin averaging or Gaussian weighting could be done, both of which would increase the predicted power.

The effect of wind turbine spacing on relative power can also be examined because the OWEZ wind plant has turbine spacings of 7.1 D, 11.1 D, 13.2 D, and 18.1 D. Figure 8 shows relative mean power for different spacings. The field data is from the 4%–6% freestream turbulence intensity bin, and the DWM model data is from a simulation with 4.5% turbulence intensity. The field data is wind-direction-bin averaged to ±1° of the row directions, and the DWM model data is Gaussian weighted and also wind-direction-bin averaged to ±1°. The DWM model generally underpredicts the power deficit of the downstream turbines, especially on the second turbine in each row. Whether or not this underprediction is truly a model inaccuracy is unclear as discussed above. However, the DWM model prediction lies will within the field data scatter. Also, the DWM

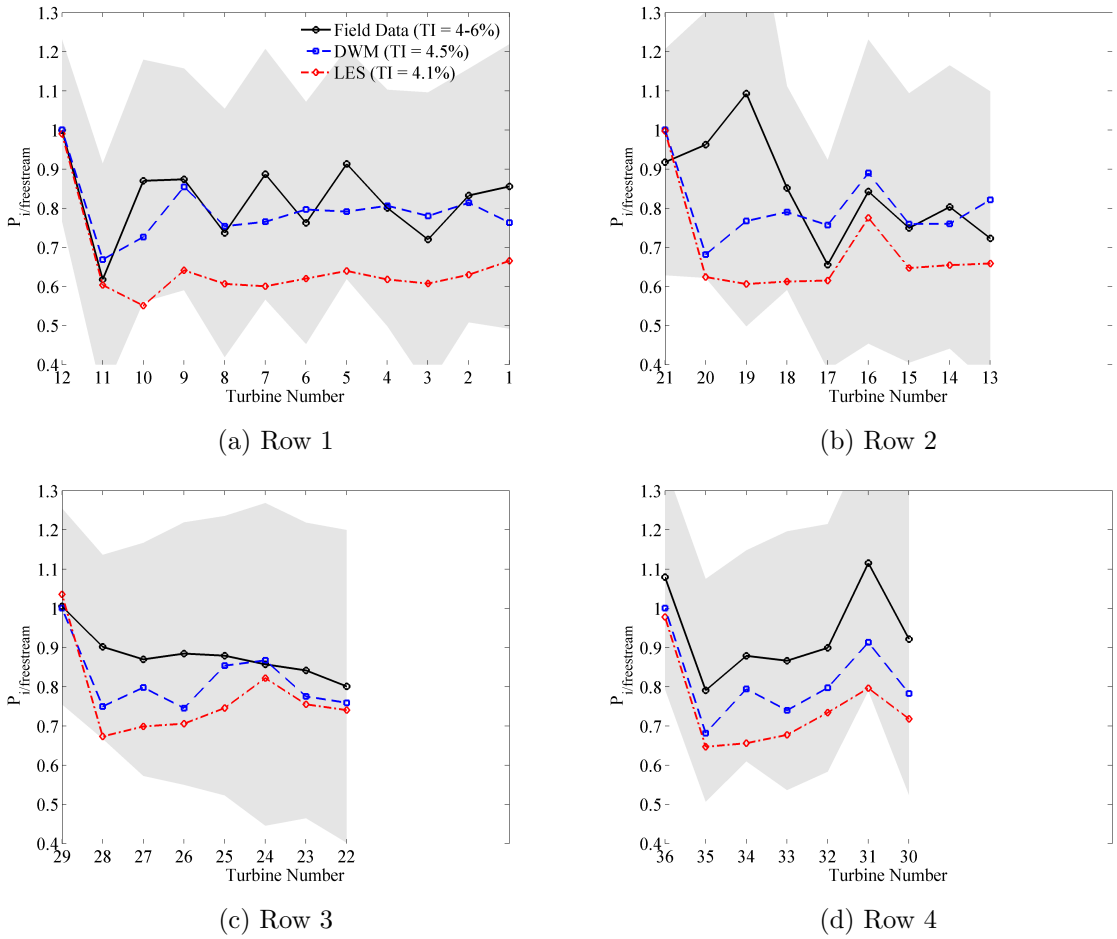

Figure 7. Mean power of each turbine in each row relative to the average of the power produced by the freestream turbines (12, 21, 29, 36). The black solid line is the bin-average (±1°) of 10-minute mean field data. The gray shading denotes ±1 standard deviation of the field data. The blue dashed line is the Gaussian-weighted and bin-averaged (±1°) 350-s mean DWM model data. The red dash-dot line is the 10-minute LES data. The wind direction is 315° and the turbulence intensity is 4%–6%.

model follows the trend of the field data in that the power deficit of the downstream turbines is decreased as spacing is increased.

Last, we examined the effect of turbulence intensity on relative mean power. We examined the 318.7° case for row 2. Figure 9 shows the mean relative power from field data and the DWM model at the five different freestream turbulence intensity levels studied. Again, the DWM model data is Gaussian weighted, and both the DWM model and field data are wind-direction-bin averaged to ±1°. There is substantial scatter in the field data as denoted by the shaded gray ±1 standard deviation area. There is also odd behavior with the data, such as in the 6%–8% turbulence intensity case in which there is a substantial overshoot in mean relative power for the third turbine in the row (turbine 19). This may be attributed to the lack of field data points which would result in unconverged mean values. In general, the field data shows higher relative power than the DWM model, but both the field data and DWM model show a general increase in relative power of waked turbines as freestream turbulence intensity increases. This occurs because elevated freestream turbulence causes enhanced wake recovery and increased wake meandering. For all cases, the shape of the DWM model-predicted profile is the same, but the profiles scales up with increased freestream turbulence intensity.

IV.B. Mechanical Loads

In this section we examine blade-root out-of-plane (BR-OOP) bending moment. This quantity is a popular choice in examining turbine structural response to its inflow because it is linked with blade fatigue, fatigue

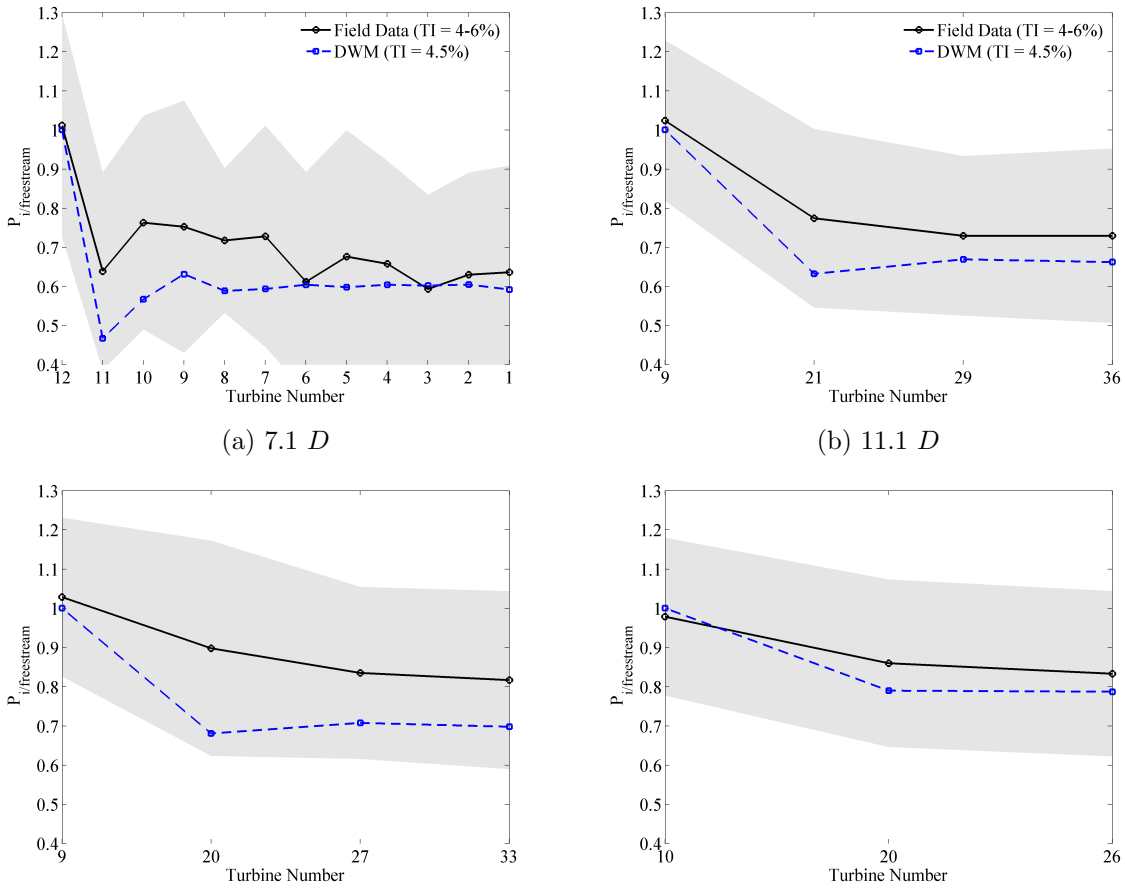

Figure 8. Effect of wind turbine spacing on mean power relative to the average of the power produced by the freestream turbines (12, 21, 29, 36). The black solid line is the bin-average (±1°) of 10-minute mean field data. The gray shading denotes ±1 standard deviation of the field data. The blue dashed line is the Gaussian-weighted and bin-averaged (±1°) 350-s mean DWM model data. The wind direction is different for each plot but row aligned such that different wind turbine spacings can be examined, and the turbulence intensity is 4%–6%.

of the connection of the blade to the hub, and it causes a non-torque moment on the main shaft if the blades are not all experiencing the same BR-OOP bending moment at the same time.

Figure 10 shows the mean BR-OOP bending moment on the blades of turbine 7 over the entire wind rose for different turbulence intensity levels and in the 8 m/s–10 m/s wind speed bin. The regions of waking are clearly indicated by decreased bending moment because the rotor experiences a lower wind speed. These plots closely follow the behavior of the wind plant efficiency shown in Figure 5. For wind directions in which the turbine spacing is greater, the minimum mean BR-OOP bending moment is higher than for closer spacings, as is expected due to increased wake recovery at greater distances. Also, elevated turbulence intensity makes the minima have higher values.

The Gaussian-weighed, wind-direction-bin averaged DWM model values generally appears to be lower than the field data for directions in which there are wake effects. This could indicate that the DWM model does not create enough wake meandering at turbines deeper into the wind plant, such as turbine 7. The meandering mechanism of the DWM model relies only on the inflow turbulent wind field to cause meandering, but our LES results visually indicate that meandering is enhanced deeper into the wind plant in which there are multiple wake interactions. This is shown in Figure 11 in which a horizontal contour plane at the turbine hub height (70 m) of instantaneous velocity computed by the LES is shown. The figure is centered about the front part of row 1, and the nature of the wake of the leading turbine is much more coherent than that of the turbines further downstream. The DWM model does not capture these multiple wake interactions, and this should be considered as an area for future improvement of that model.

The single LES computation at 315° at an inflow turbulence intensity of 4.1% lies well within the scatter

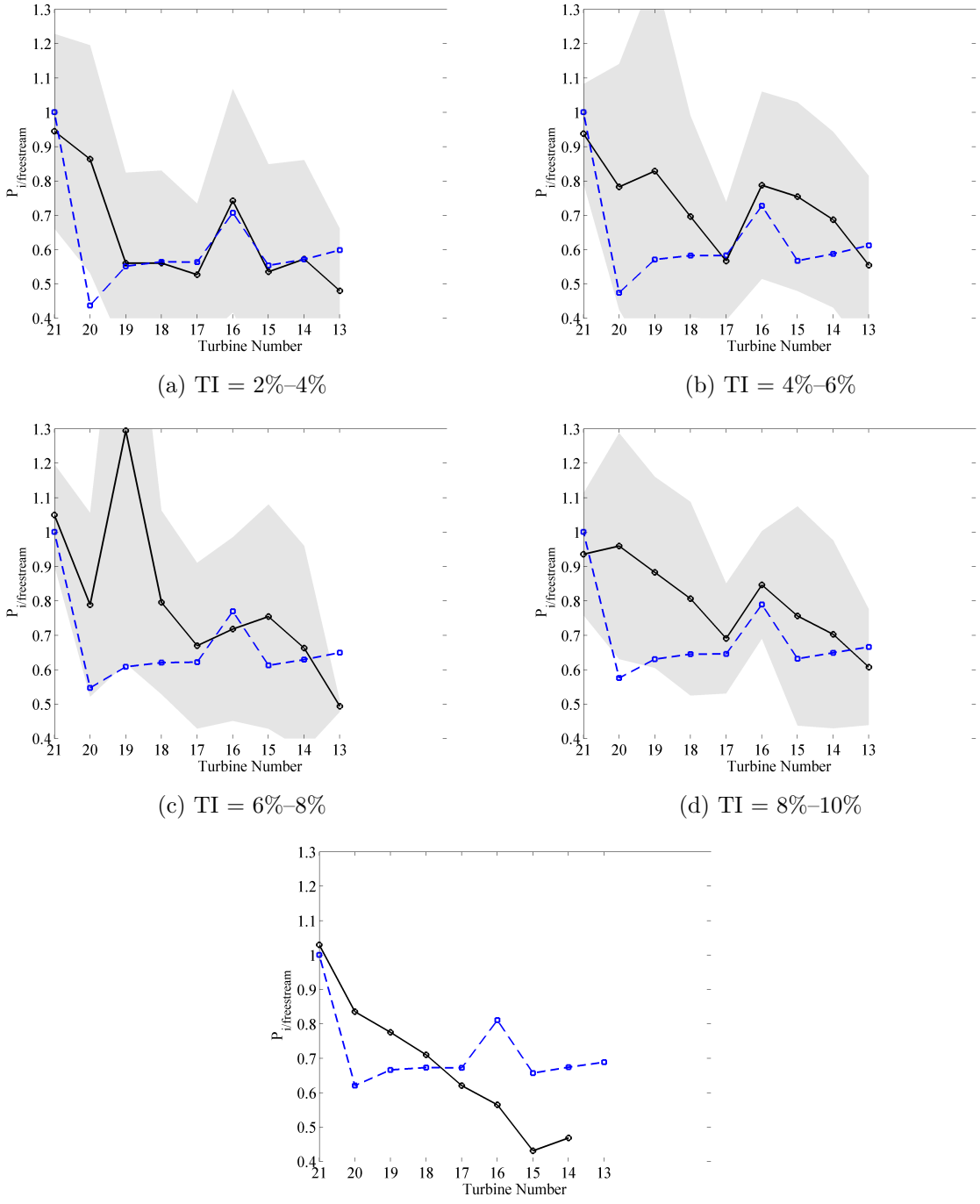

(a) TI = 2%–4%

(b) TI = 4%–6%

(c) TI = 6%–8%

(d) TI = 8%–10%

(d) TI = 10%–12%

Figure 9. Effect of turbulence intensity on mean power relative to the average of the power produced by the freestream turbines (12, 21, 29, 36). The black solid line is the bin-average ($\pm 1^\circ$) of 10-minute mean field data. The gray shading denotes ± 1 standard deviation of the field data (the plot in (d) does not have the gray area because there is not enough data at that turbulence intensity range to create a reliable standard deviation). The blue dashed line is the Gaussian-weighted and bin-averaged ($\pm 1^\circ$) 350-s mean DWM model data. The wind direction is row aligned at 318.7°.

of the field data and agrees well with the Gaussian-weighted and wind-direction-bin-averaged DWM model prediction.

Although the mean BR-OOP bending moment is informative, the root-mean-square (RMS) BR-OOP bending moment is arguably more important. The RMS is an indicator of unsteadiness in the moment, and hence an indicator of fatigue that is damaging to turbine components. We found it most useful to

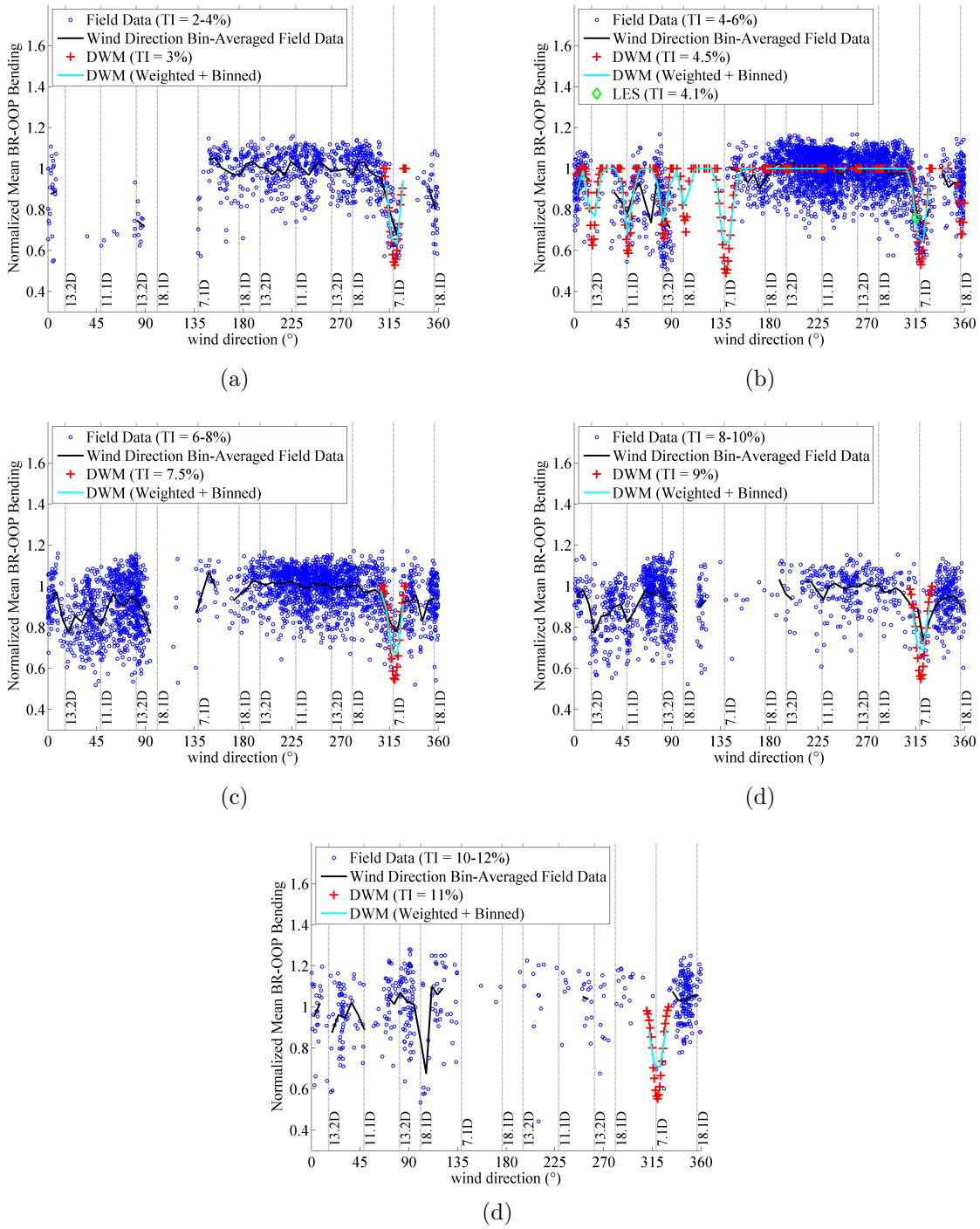

Figure 10. Plots of turbine 7 freestream normalized mean blade-root out-of-plane bending moment versus wind direction for different turbulence intensity levels.

examine RMS BR-OOP bending moment of turbine 7 normalized by its RMS BR-OOP bending moment when subject to free, non-waked atmospheric inflow from the southwest quadrant. As freestream turbulence intensity increases, so does RMS BR-OOP bending moment of turbine 7 when it is not waked. When it is waked, both the unsteadiness of the wake and the freestream turbulence affect the RMS moment. By normalizing by the freestream RMS moment, the effect of freestream turbulence on the RMS moment is removed, and only the effect of the wake is seen.

Figure 12 shows freestream normalized RMS BR-OOP bending moment of turbine 7. The field data is

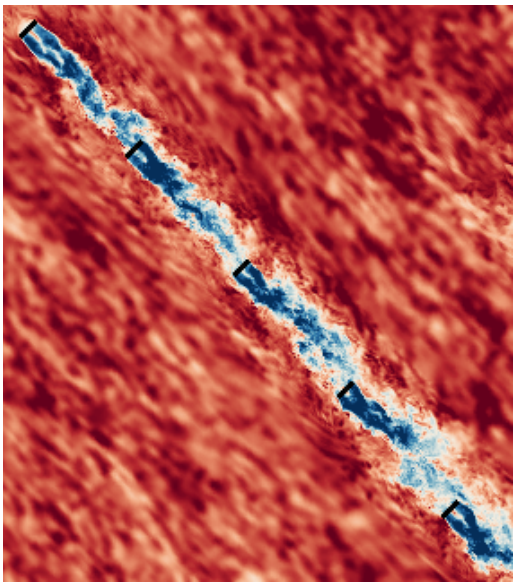

Figure 11. A horizontal contour plane at the turbine hub height of 70 m showing the instantaneous velocity field from the LES. This view is centered around the front of row 1 (turbines 12–8). Red (blue) colors denote low (high) velocity magnitude. Flow is from the upper left (northwest).

based on 10-minute samples, the DWM model data is based on 350-s samples, and the LES data is based on a 10-minute sample. The DWM model data is Gaussian weighted in an attempt to replicate the wind-direction uncertainty of the field data, and wind-direction-bin averaged to ±2.5° as with the field data.

There are clear peaks in normalized RMS BR-OOP bending moment for directions in which waking is present. The best examples are the 4%–6% and 6%–8% turbulence intensity ranges. The 318.7° direction with the small 7.1 D spacing shows a peak in which the individual field data points show RMS moments between 2 and 6 times as great as the freestream RMS moments depending on turbulence intensity of the freestream. The DWM model somewhat overestimates these values showing individual peak values 2.5 to 6.5 times greater than the freestream values. The bin averaged RMS moment peaks from the DWM model are also 2 to 3 times greater than those of the field data. It is unclear if the DWM model is truly overpredicting the RMS BR-OOP bending moment so dramatically or not. It is possible that because the DWM model does not capture the effects of multiple wake interactions that it could be in error. However, there is much uncertainty in the inflow that could be causing this discrepancy. There is uncertainty in the wind direction measurement, which we have discussed in depth. There is also uncertainty in what a certain turbulence intensity level means in the field data. For example, using 10-minute statistics as was done with the OWEZ field data, an inflow with a fixed mean wind direction and a certain level of turbulence may appear the same as an inflow with a gradually sweeping wind direction and lower turbulence intensity. The case with the gradually sweeping wind direction would likely cause lower RMS BR-OOP bending moment values on wake turbines. The single LES data point is within the scatter of the individual field data points but on the high end of the scatter.

Figure 13 compares the freestream normalized RMS BR-OOP bending moment of every turbine as computed with the DWM model and LES for the 315° wind direction, which is slightly oblique to the main row direction. Field data are not shown because they were only measured on turbines 7 and 8. The turbulence intensity levels for each simulation are similar, 4.5% for the DWM model and 4.1% for the LES. However, the differences are significant. The DWM model predicts values that are up to 1.7 times higher than those of the LES for turbines at least 4 positions into the wind plant. It is unclear why the two models predict freestream normalized RMS BR-OOP levels so differently, but it could be that the freestream non-normalized values are different. The DWM model uses a stochastically generated turbulent inflow field but the LES uses an inflow generated from a separate precursor LES. Stochastic versus precursor LES inflow generation methods are very different. Although the turbulence intensities are similar, the nature of the turbulence in the two cases may be very different. We plan to feed the same precursor-generated LES inflow into the DWM model and see how this changes the loads.

In Figure 14, we examine only the DWM model results of freestream normalized RMS BR-OOP on

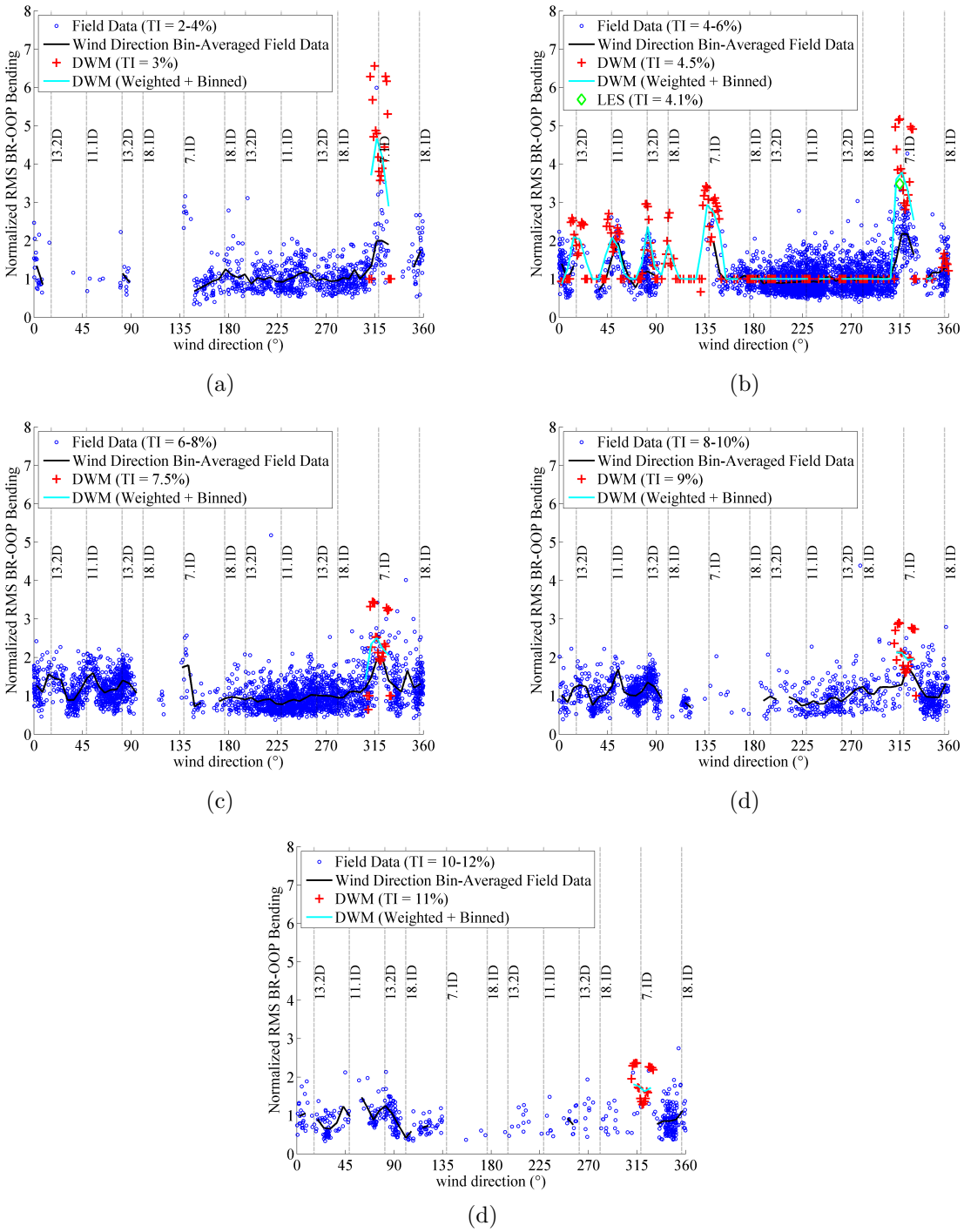

Figure 12. Plots of turbine 7 RMS blade-root out-of-plane bending moment (normalized by freestream RMS values) versus wind direction for different turbulence intensity levels.

turbine 7. We specifically look at a narrow wind direction sector centered on the 7.1 D spacing direction of 318.7° and the effect of freestream turbulence intensity. A main feature of the RMS BR-OOP profiles is that there is a peak on either side of row-aligned winds. We expected this because those peaks coincide with partial waking situations in which the rotor blade flies in and out of the wake, creating large BR-OOP fluctuations. This is likely not observed in the field data because of the wind-direction uncertainty. We also see that the DWM model predicts that as the freestream turbulence intensity is increased, the normalized RMS BR-OOP levels decrease for waking wind direction. For example, at 3% turbulence intensity, the peak

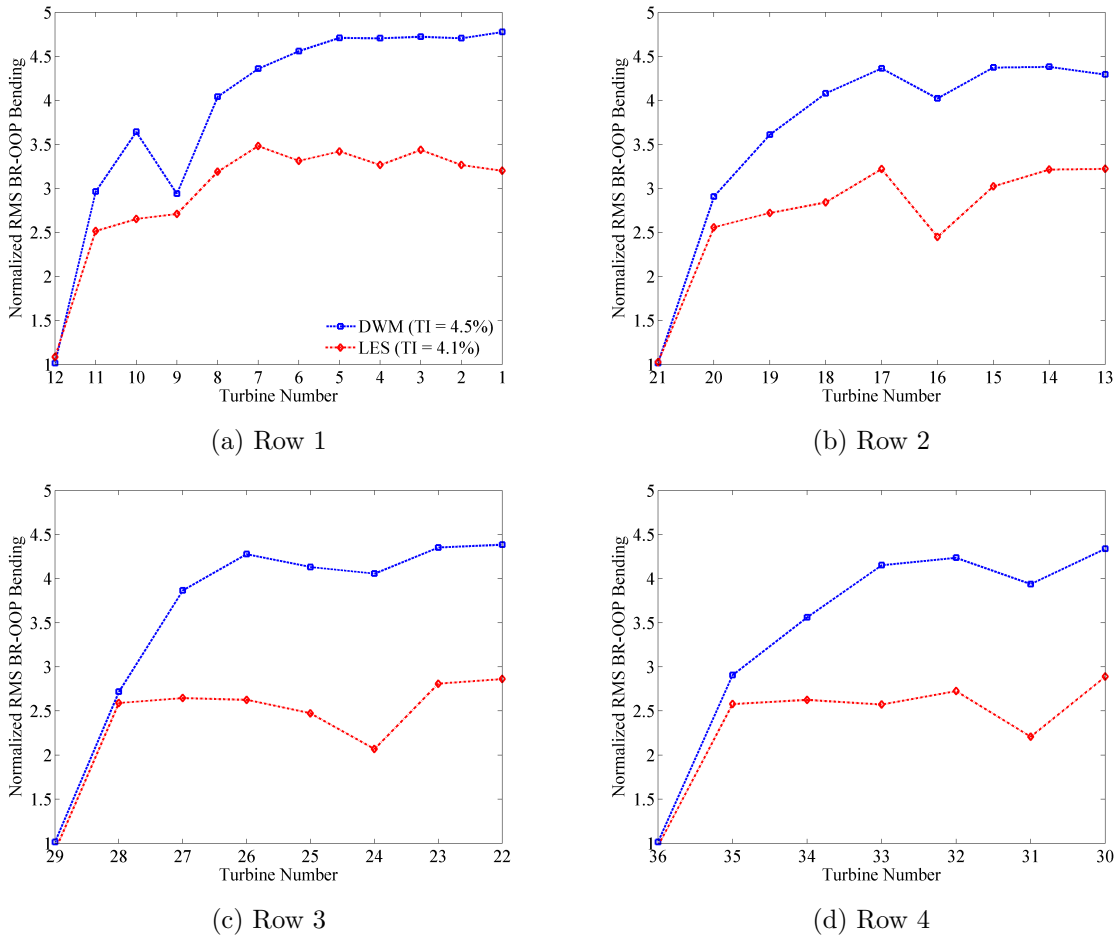

(a) Row 1 (b) Row 2

(c) Row 3 (d) Row 4

Figure 13. Plots of RMS blade-root out-of-plane bending moment (normalized by freestream RMS values) for each of the four main rows as computed with the DWM model and LES. The wind direction is slightly oblique to the row at 315°. For the DWM model and LES data, the freestream turbulence intensity is 4.5% and 4.1%, respectively.

RMS BR-OOP is roughly 6.5 times its freestream level, but at 11% turbulence intensity, its peak value is about 2.25 times its freestream level.

IV.C. Calculation Cost

The DWM model and LES have dramatically different computational costs. The DWM model simulations were run on a desktop computer with two 2.0 GHz cores. One-hundred different 350-s DWM model simulations of the entire OWEZ wind plant required roughly 48 central-processing-unit-hours (CPU-hrs) on this desktop. In contrast, a single equivalent LES of the entire OWEZ wind plant requires 280,000 CPU-hrs on a high-performance computing system. It is important to note that when we performed the LES, we were outputting a lot of data in the form of various sample planes of the flow field at fairly high frequency, and the time spent writing to disk was significant. Without this large amount of data output, the compute time requirement may have been been reduced by a third, which is still six orders of magnitude different than the DWM model computational cost.

V. Conclusions and Future Work

In this study, we compared the DWM model, LES, and field data for the 36-turbine, 108-MW OWEZ offshore wind plant. There is a wealth of field data from OWEZ that consists of meteorological mast readings, SCADA data from every turbine, and strain-gauge measurements from two of the turbines. The field data was collected over a period of 3 years and 10-minute statistics are given. The field data shows

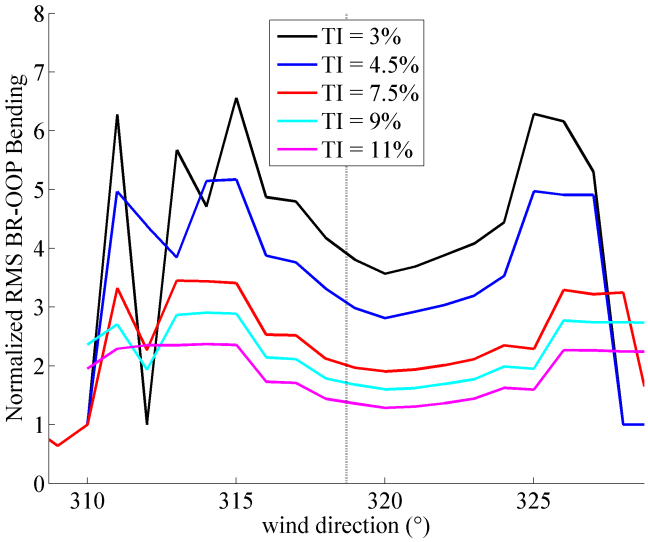

Figure 14. DWM model simulated turbine 7 RMS blade-root out-of-plane bending moment (normalized by freestream RMS values) versus wind direction for different turbulence intensity levels centered about the 318.7° row direction (shown as a vertical dotted line).

clear dependence of power and mechanical loads on waking and turbulence intensity. The wind plant has multiple row directions with different spacing, and the effect of different spacing is evident.

We were only able to run one LES case because of its high cost combined with time constraints. The computational mesh required 308 million cells with a finest resolution around the turbines and their wakes of 1.5 m. We were able to run many different situations with the DWM model because of its much lower cost. We simulated the entire wind rose for the 4%–6% turbulence intensity case, and for the remaining 4 different freestream turbulence intensities, we simulated a sector around the main row direction of 318.7° which has a spacing of 7.1 D.

Both the DWM model and LES appear to underpredict the power produced by downstream waked turbines. However, it is unclear if the underprediction is due to model inaccuracy or uncertainty in the field data. The underprediction still lies within one standard deviation of the field data from its wind-direction bin average. We tried to account for wind-direction uncertainty by applying a Gaussian-weighted average of values in a small sector centered upon the direction of interest following the work of Gaumond et al.[21]

The DWM model greatly overpredicts RMS BR-OOP moments compared to the field data and to LES. Because the DWM model and LES are not in agreement in terms of RMS loads, it seems that the DWM model is not capturing some aspect of wake meandering that occurs deeper into a wind plant when multiple wakes merge. We saw clear differences in the meandering behavior of turbines deep in the farm as compared to the leading turbines in the LES data. The DWM model has a very simple meandering model, and it could need to be enhanced to account for multiple wake merging behavior.

Some of the differences between the DWM model and the LES may arise from the the different inflow generation methods used in each model. A stochastic inflow turbulence generator was used for the DWM model, but a precursor atmospheric LES created the inflow for the wind plant LES. These two methods may produce turbulence fields with similar turbulence intensities, but the nature of the turbulence in each case may be quite different. In future work, we plan to feed the LES precursor-generated inflow into the DWM model to see if this is the cause for some of the differences between the DWM model and LES results.

This study highlights the difficulty in comparing simulation and field data. The simulations consist of only one realization of each different wind direction and turbulence level. The field data was collected over 3 years, so many data points may be averaged within the same direction, speed, and freestream turbulence bin. There is also considerable wind-direction uncertainty in the field data that cannot be removed and is difficult to replicate in the simulations. The field data is also based on 10-minute averages. Two very different wind conditions may yield the same 10-minute mean wind speed, direction, and turbulence intensity. There is clearly a need for field data that is not based on 10-minute averages, but based on time histories of a sufficient sampling frequency to truly understand what conditions created the 10-minute statistics.

In the future, we plan to run more LES cases. We may possibly run abbreviated versions of the wind plant to cut down on computational cost to allow for more conditions to be simulated. We will use the meandering information from the LES to improve the DWM model.

Although detailed comparison with field data is difficult, from a broader perspective, the DWM model results are promising. The overall wake effects on performance seen in the field data are reproduced by the DWM model, which is many orders of magnitude less costly than LES. With further enhancements and improvements through more comparisons with field data and LES, the DWM model will likely evolve into a workhorse wind plant aerodynamics tool that could potentially replace models like the Park and eddy-viscosity wake models and current standards for wake turbulence.

Acknowledgments

This work was supported by the U.S. Department of Energy (DOE) under Contract No. DE-AC36-08GO28308 with the National Renewable Energy Laboratory. Funding for the work was provided by the DOE Office of Energy Efficiency and Renewable Energy, Wind and Water Power Technologies Office. We thank NordzeeWind for providing the invaluable OWEZ field data set. The large-eddy simulation was performed on the National Renewable Energy Laboratory's Peregrine high-performance computing system. Matt Bidwell and Kevin Regimbal of NREL provided useful assistance in the use of Peregrine. We thank Dick Veldkamp of Vestas Wind Systems for the coordination of data sharing and his useful discussion. Senu Sirnivas of NREL helped us in properly modeling the turbine model in FAST. Sang Lee of NREL provided useful discussion in the implementation of the dynamic wake meandering model.

References

[1]Larsen, G. C., Madsen, H. A., Bingöl, F., Mann, J., Ott, S., Sørensen, J. N., Okulov, V., Troldborg, N., Nielsen, M., Thomsen, K., Larsen, T. J., and Mikkelsen, R., "Dynamic Wake Meandering Modeling," Tech. Rep. R-1607(EN), Risø National Laboratory, Technical University of Denmark, Roskilde, Denmark, 2007.

[2]Larsen, G. C., Madsen, H. A., Thomsen, K., and Larsen, T. J., "Wake Meandering – A Pragmatic Approach," *Wind Energy*, Vol. 11, No. 4, 2008, pp. 377–395.

[3]Jensen, N. O., "A Note on Wind Generator Interaction," Tech. Rep. M-2411, Risø National Laboratory, Roskilde, Denmark, 1983.

[4]Katíc, I., Højstrup, J., and Jensen, N. O., "A Simple Model for Cluster Efficiency," *Proceedings of European Wind Energy Association Conference and Exhibition, Rome, Italy*, 1986.

[5]Ainslee, J. F., "Calculating the Flowfield in the Wake of Turbines," *Journal of Wind Engineering and Industrial Aerodynamics*, Vol. 27, 1985, pp. 213–224.

[6]Bingöl, F., Mann, J., and Larsen, G., "Light Detection and Ranging Measurements of Wake Dynamics, Part I: One-Dimensional Scanning," *Wind Energy*, Vol. 13, 2010, pp. 51–61.

[7]Trujillo, J.-J., Bingöl, F., Larsen, G., Mann, J., and Kühn, M., "Light Detection and Ranging Measurements of Wake Dynamics, Part II: Two-Dimensional Scanning," *Wind Energy*, Vol. 14, 2011, pp. 61–75.

[8]"International Electrotechnical Commission (IEC) International Standard 61400-1, 3rd Edition, Wind Turbines," International Electrotechnical Commission, Reference Number: IEC 61400-1:2005(E).

[9]Larsen, T. J., Madsen, H. A., Larsen, G. C., and Hansen, K. S., "Validation of the Dynamic Wake Meandering Model for Loads and Power Production in the Egmond aan Zee Wind Farm," *Wind Energy*, Vol. 16, No. 4, 2012, pp. 605–624.

[10]Jonkman, J., "FAST – An Aeroelastic Computer-Aided Engineering Tool for Horizontal Axis Wind Turbines," available online at http://wind.nrel.gov/designcodes/simulators/fast, accessed June 2, 2014, created by National Renewable Energy Laboratory.

[11]Hao, Y., Lackner, M. A., Keck, R.-E., Lee, S., Churchfield, M. J., and Moriarty, P., "Implementing the Dynamic Wake Meandering Model in the NWTC Design Codes," *Proceedings of 32nd ASME Wind Energy Symposium, National Harbor, Maryland*, AIAA, Wahington, DC, 2014, AIAA Paper 2014-1089.

[12]Churchfield, M. and Lee, S., "Simulator for Wind Farm Applications (SOWFA)," available online at http://wind.nrel.gov/designcodes/simulators/sowfa, accessed June 2, 2014, created by National Renewable Energy Laboratory.

[13]Keck, R.-E., de Maré, M., Churchfield, M. J., Lee, S., Larsen, G., and Madsen, H. A., "Two Improvements to the Dynamic Wake Meandering Model: Including the Effects of Atmospheric Shear on Wake Turbulence and Incorporating Turbulence Build-up in a Row of Wind Turbines," *Wind Energy*, 2013, Published online in Wiley Online Library.

[14]Kelley, N. and Jonkman, B., "TurbSim – A Stochastic, Full-Field, Turbulent-Wind Simulator," available online at http://wind.nrel.gov/designcodes/preprocessors/turbsim, accessed June 2, 2014, created by National Renewable Energy Laboratory.

[15]Churchfield, M. J., Lee, S., Michalakes, J., and Moriarty, P. J., "A Numerical Study of the Effects of Atmospheric and Wake Turbulence on Wind Turbine Dynamics," *Journal of Turbulence*, Vol. 13, No. 14, 2012.

[16]OpenCFD Ltd. (ESI Group), "OPENFOAM – The Open Source CFD Toolbox," available online at http://www.openfoam.com, accessed June 2, 2014.

[17]Meneveau, C., Lund, T., and Cabot, W., "A Lagrangian Dynamic Subgrid-Scale Model of Turbulence," *Journal of Fluid Mechanics*, Vol. 319, 1996, pp. 353–385.

[18]Sørensen, J. N. and Shen, W. Z., "Numerical Modeling of Wind Turbine Wakes," *Journal of Fluids Engineering*, Vol. 124, 2002, pp. 393–399.

[19]Churchfield, M. J., Lee, S., Moriarty, P. J., Martínez, L. A., Leonardi, S., Vijayakumar, G., and Brasseur, J. G., "A Large-Eddy Simulation of Wind-Plant Aerodynamics," *50th AIAA Aerospace Sciences Meeting including the New Horizons Forum and Aerospace Exposition, Nashville, TN, Jan. 9–12, 2012*, AIAA, Washington D.C., 2012, AIAA Paper 2012-537.

[20]Kelley, N. D., "Turbulence-Turbine Interaction: The Basis for the Development of the TurbSim Stochastic Simulator," Tech. Rep. NREL/TP-5000-52353, National Renewable Energy Laboratory, Golden, Colorado, 2011.

[21]Gaumond, M., Réthoré, P.-E., Ott, S., Peña, A., Bechmann, A., and Hansen, K. S., "Evaluation of the wind direction uncertainty and its impact on wake modeling at the Horns Rev offshore wind farm," *Wind Energy*, Vol. 17, 2014, pp. 1169–1178.